Supporting Information

Tracking Charge Transfer to Residual Metal Clusters in Conjugated Polymers for Photocatalytic Hydrogen Evolution

Michael Sachs,[1] Hyojung Cha,[1] Jan Kosco,[2] Catherine M. Aitchison,[3] Laia Francàs,[1] Sacha Corby,[1] Chao-Lung Chiang,[4] Anna A. Wilson,[1] Robert Godin,[1†] Alexander Fahey-Williams,[1] Andrew I. Cooper,[3] Reiner Sebastian Sprick,[3*] Iain McCulloch[2*] and James R. Durrant[1*]

1 Department of Chemistry and Centre for Processable Electronics, Imperial College London, 80 Wood Lane, London W12 0BZ, U.K.

2 Department of Physical Sciences and Engineering, KAUST Solar Centre (KSC), 4700 KAUST, 23955 Thuwal, Saudi Arabia.

3 Department of Chemistry and Materials Innovation Factory, University of Liverpool, 51 Oxford Street, Liverpool L7 3NY, U.K.

4 National Synchrotron Radiation Research Center, 101 Hsin-Ann Rd., Hsinchu 30076, Taiwan.

1. P3HT hydrogen evolution experiments

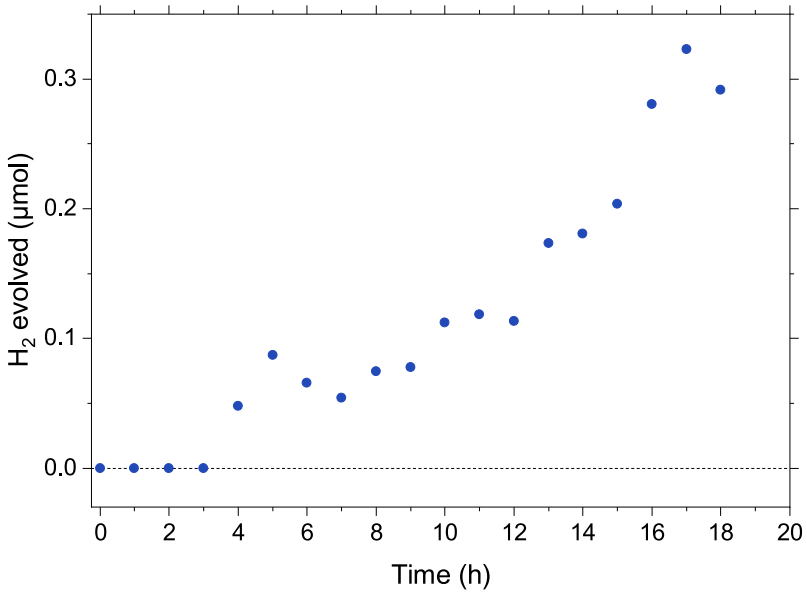

Figure S1. Hydrogen evolution experiment using P3HT nanoparticles with a 40 nm diameter and 5 wt. % photodeposited Pt in a 1:1:1 H_2O/methanol/triethylamine mixture, irradiated by the output of a 300 W xenon lamp (385 - 700 nm). Note that the hydrogen evolution activity of P3HT is very low and in fact close to the resolution limit of our instrument, therefore there is visible noise in this P3HT HER data.

2. F8BT exciton diffusion length measurements

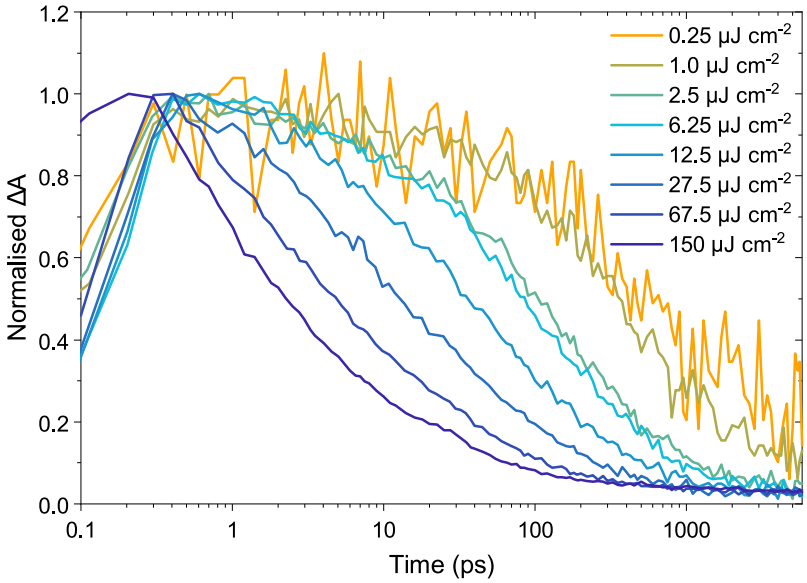

Figure S2. Transient absorption decay kinetics of F8BT nanoparticles with <1 ppm Pd in aqueous suspension probed at 950 nm following 460 nm excitation with excitation fluences of 0.25 – 150 μJ cm^{-2}.

Table S1. Parameters for diffusion length calculation by exciton-exciton annihilation: excitation density n_0, half-lifetime $t_{1/2}$, intrinsic exciton lifetime constant k, relative lifetime quenching constant α, bimolecular decay rate coefficient γ, diffusion coefficient D, diffusion length L_d.

Fluence (μJ cm^{-2})	**n_0 (cm^{-3})**	**$t_{1/2}$ (ps)**	**k**	**α**	**γ**	**D (cm^2 s^{-1})**	**L_d (nm)**
1	3.45×10^{17}	370 (t_0)	1.87×10^{9}				
2.5	8.63×10^{17}	104	1.87×10^{9}	0.28	7.93×10^{-9}	2.19×10^{-3}	9.0
12.5	4.31×10^{18}	33	1.87×10^{9}	0.090	6.38×10^{-9}	1.76×10^{-3}	8.1
27.5	9.49×10^{18}	12	1.87×10^{9}	0.032	8.49×10^{-9}	2.35×10^{-3}	9.3
67.5	2.33×10^{19}	4.3	1.87×10^{9}	0.012	9.87×10^{-9}	2.73×10^{-3}	10.0
150	5.18×10^{19}	2.2	1.87×10^{9}	0.0059	8.73×10^{-9}	2.41×10^{-3}	9.5
				Average	**8.28×10^{-9}**	**2.29×10^{-3}**	**9.2**

Calculation of exciton diffusion lengths via singlet exciton−singlet exciton annihilation (EEA)

Femtosecond-transient absorption data obtained from F8BT nanoparticles (<1 ppm Pd, ~62 nm diameter) upon excitation with various fluences (1 – 150 μJ cm^{-2}), and was used to calculate the diffusion length of F8BT excitons in the absence of Pd. The model used assumes that exciton decay via radiative and non-radiative deactivation with intrinsic exciton decay rate constant (k) and via bimolecular EEA[1–3] with a bimolecular decay rate coefficient (γ), as shown in Equation S1, where n(t), in cm^{-3} is the exciton density at a given delay time t after laser excitation,

$$-\frac{dn(t)}{dt} = kn + \gamma n^2 \qquad \text{(Eq. S1)}$$

$$n(t) = \frac{n_0\, exp(-kt)}{1+(\gamma/k)n_0[1-exp(-kt)]} \quad \text{(Eq. S2)}$$

A useful indication of the rate of a first-order chemical reaction is the half-life time $t_{1/2}$ of photo-generated excitons, i.e. the time after which the exciton population has decayed to half of its initial value.

The time for $n(t)$ to decrease from n_0 to $\frac{1}{2}\, n_0$ in a first-order reaction is given by

$$t_{1/2} = \frac{ln\, 2}{k} \quad \text{(Eq. S3)}$$

$t_{1/2}$ at the lowest fluence is referred to as t_0 here, meaning $t_{1/2} = t_0 = \frac{ln\, 2}{k}$, which yields $k = 1.87\times10^9$.

On the other hand, at higher fluences, $t_{1/2} = \alpha t_0 = \frac{\alpha\, ln\, 2}{k}$, when α <1.

We can then rearrange this Eq. S2 using the half-life time of the exciton decay,

$$\frac{n(t)}{n_0} = \frac{exp(-kt_{1/2})}{1+(\gamma/k)n_0[1-exp(-kt_{1/2})]} = \frac{1}{2} \quad \text{at } t=t_{1/2} \quad \text{(Eq. S4)}$$

It follows that

$$exp(-kt_{1/2}) = \frac{1+\frac{\gamma}{k}n_0}{2+\frac{\gamma}{k}n_0} \quad \text{(Eq. S5)}$$

By substituting $t_{1/2} = \frac{\alpha\, ln\, 2}{k}$,

$$\gamma = \frac{k(2\, exp(-\alpha\, ln\, 2)-1)}{n_0(1-exp(-\alpha\, ln\, 2))} \quad \text{(Eq. S6)}$$

If α is low enough, $exp(-\alpha\, ln\, 2) = 1 - \alpha\, ln\, 2$. Hence

$$\gamma = \frac{k(2-2\alpha\, ln\, 2-1)}{n_0\alpha\, ln\, 2} = \frac{k}{n_0\alpha\, ln\, 2} = \frac{1}{n_0 t_{1/2}} \quad \text{(Eq. S7)}$$

The modified EEA bimolecular decay rate coefficient was obtained from Eq. S6 and was calculated to be to be $\gamma = 7.93\times10^{-9}$ cm^3 s^{-1} at a fluence of 2.5 μJ/cm^2.

$$\gamma = 4\pi R_a D \quad \text{(Eq. S8)}$$

We used an annihilation radius R_a = 2.88 nm corresponding to the distance at which singlet-singlet exciton annihilation is faster than exciton diffusion. $D = 2.29\times10^{-3}$ cm^2 s^{-1} was obtained by using Equation S8.[1–3]

The exciton diffusion length (L_d) of 9.2 nm can be calculated using,

$$L_d = \sqrt{D \cdot \tau} \quad \text{(Eq. S9)}$$

3. F8BT fs-ns TAS

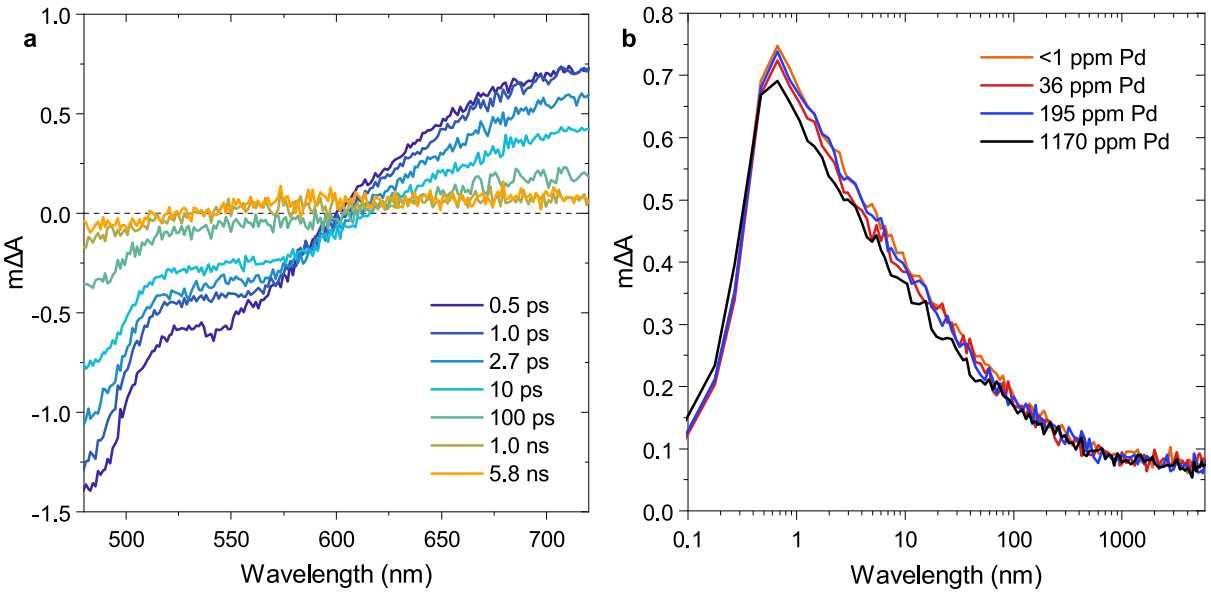

Figure S3. fs-ns transient absorption data of F8BT nanoparticles suspended in H_2O. **(a)** Spectra probed at the indicated times for F8BT (< 1 ppm Pd), and **(b)** kinetics probed at 700 nm for different Pd concentrations. All data was acquired at an excitation wavelength of 460 nm and a fluence of 16.5 μJ cm^{-2}. All suspensions were prepared with an absorbance of 0.20 at the excitation wavelength to ensure a constant number of absorbed photons.

The transient absorption spectra probed before 1 ns shown in Figure S3a exhibit a negative ΔA signal below 610 nm, which can be assigned to a mixture of ground state bleach and stimulated emission. The positive signal above 610 nm is assigned to excited state absorption of photogenerated excitons, and this signal can therefore be used to track the exciton population. Figure S3a shows the decay kinetics probed at 700 nm for aqueous nanoparticle dispersions with different Pd contents. We estimate that 10% of photogenerated excitons are quenched by Pd before 100 fs (the time resolution of the instrument) in 1170 ppm F8BT compared to <1 ppm Pd F8BT based on the initial signal amplitude.

4. F8BT exciton quenching in H2O vs. 30 vol. % DEA

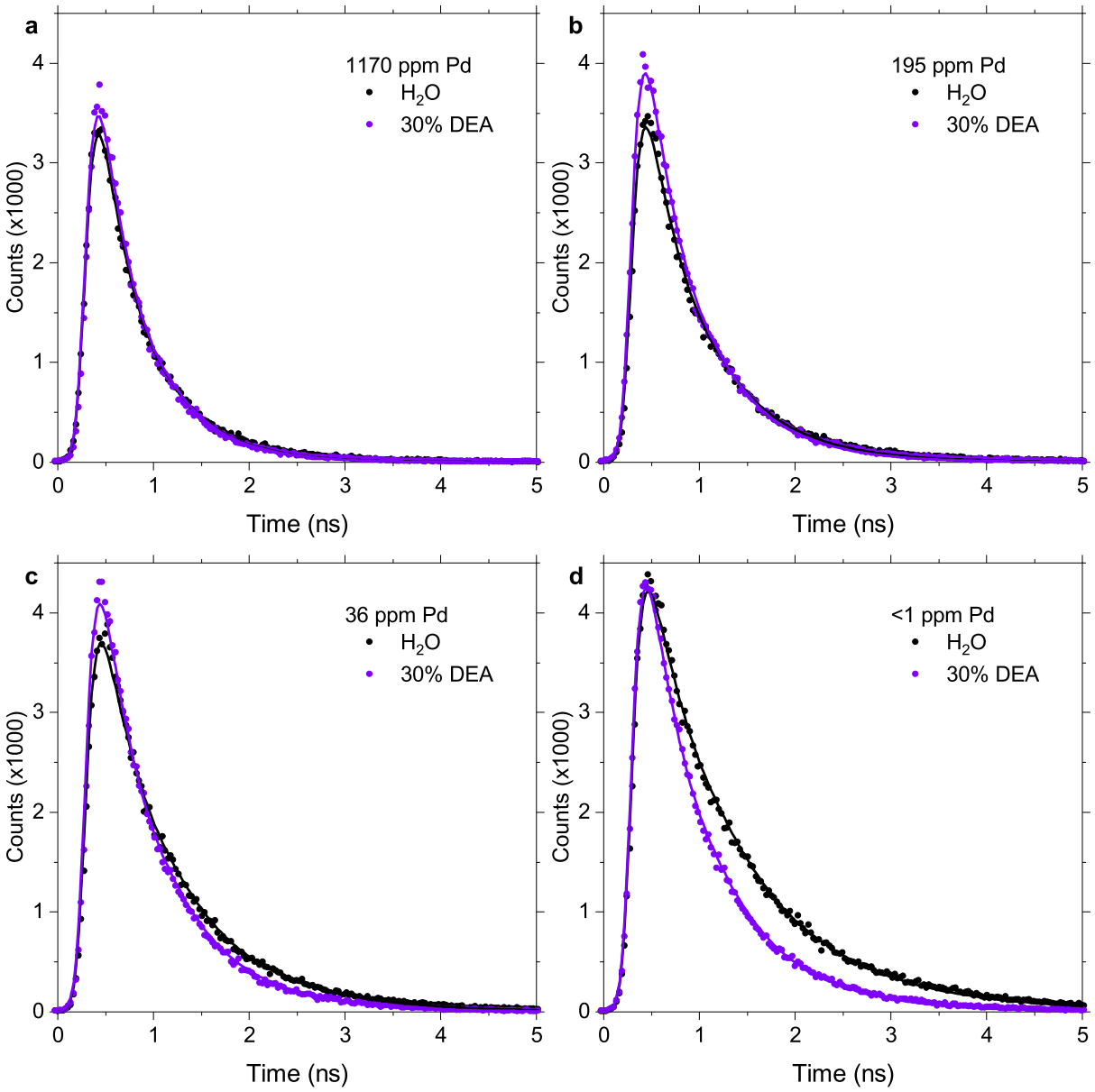

Figure S4. Photoluminescence decays of F8BT nanoparticle suspensions in H_2O and in a 30 vol. % DEA in H_2O mixture, probed at 545 nm upon 465 nm excitation, for different Pd concentrations: **(a)** 1170 ppm, **(b)** 195 ppm, **(c)** 36 ppm, **(d)** <1 ppm. All suspensions were prepared with an absorbance of 0.10 at the excitation wavelength to ensure a constant number of absorbed photons and emitted photons were counted over a time period of 10 s. We note that an increase in the initial signal amplitude is observed for a-c in the sample with DEA, which we attribute to the evaporation of some of the relatively volatile DEA during the argon purge before the measurement. The full lines represent fits to the data obtained using iterative reconvolution of the measured instrument response and a stretched exponential function $y \propto \exp(-kt^b)$ with a stretching exponent b = 0.87.

5. Exciton quenching in F8BT nanoparticles with different sizes

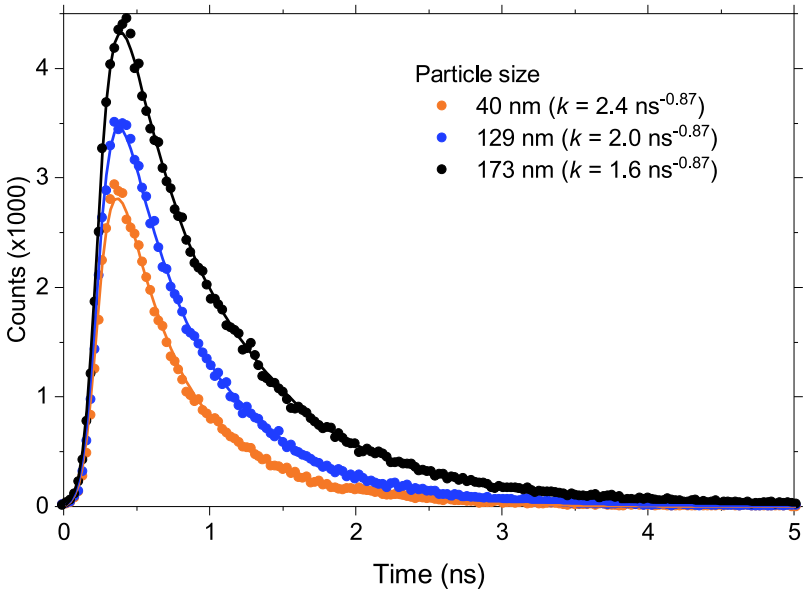

Figure S5. Photoluminescence decays of unpurified F8BT nanoparticles of different sizes suspended in H_2O, probed at 545 nm upon 467 nm excitation. All suspensions were prepared with an absorbance of 0.05 at the excitation wavelength to ensure an equal number of absorbed photons. The full lines represent fits to the data obtained using iterative reconvolution of the measured instrument response and a stretched exponential function $y \propto \exp(-kt^b)$ with a stretching exponent b = 0.87. We note that the decays in the presence of DEA follow the same trend, further demonstrating that quenching via Pd dominates quenching via DEA in unpurified F8BT (as seen in Figure S4).

6. TEM images

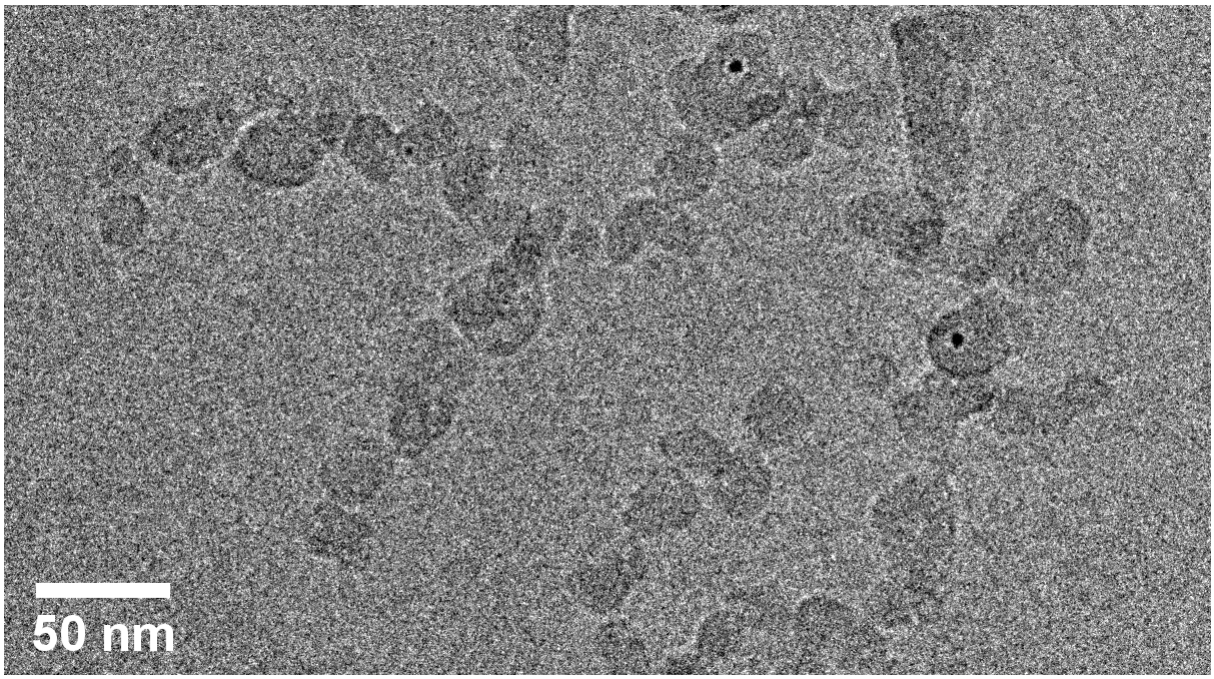

Figure S6. TEM image of F8BT nanoparticles with 1170 ppm Pd.

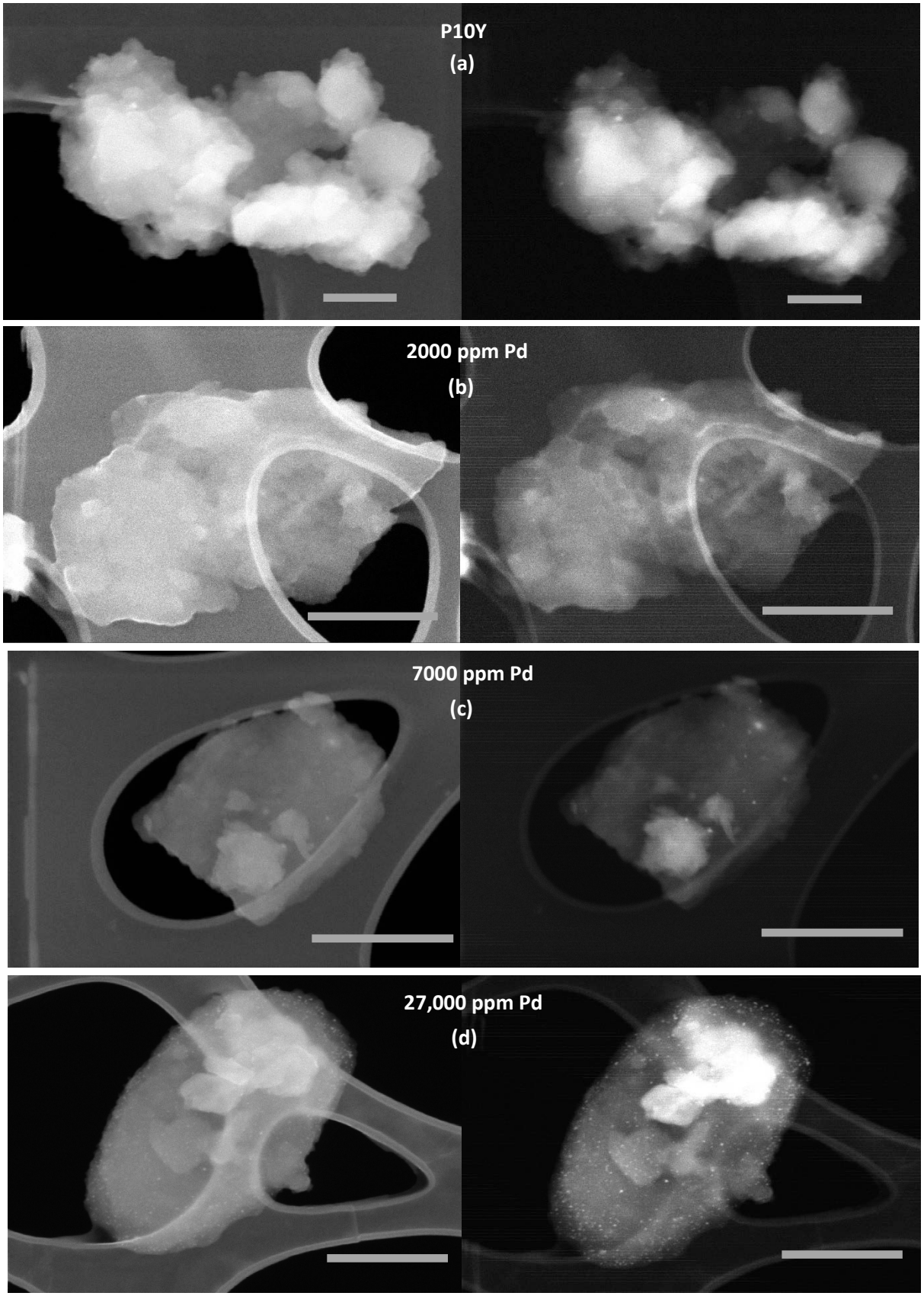

Figure S7. SEM (left) and HADF STEM (right) images of **(a)** P10Y and Suzuki-Miyaura P10 with **(b)** 2000 ppm, **(c)** 7000 ppm, and **(d)** 27,000 ppm Pd. All scalebars are 500 nm.

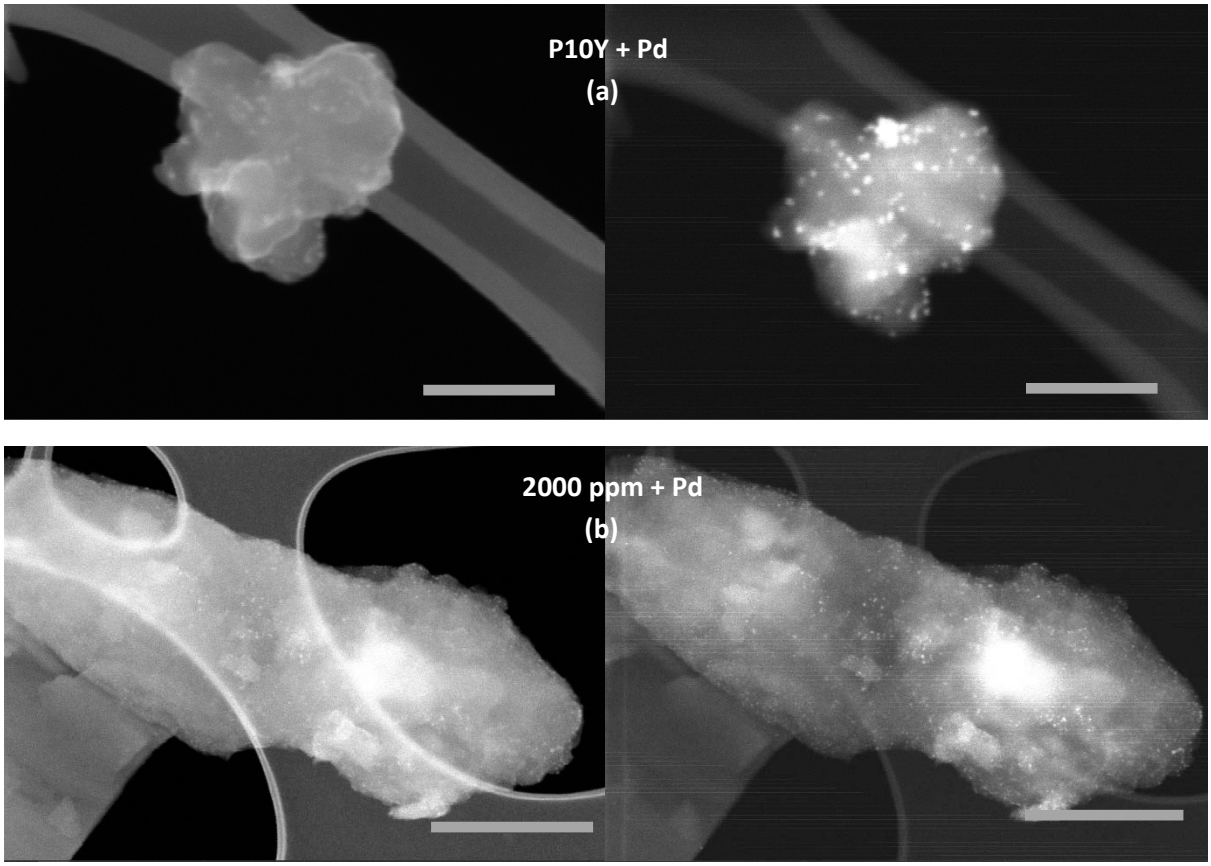

Figure S8. SEM (left) and HADF STEM (right) images of P10 particles with added Pd by in-situ photodeposition showing **(a)** P10Y + Pd and **(b)** 2000 ppm Pd + Pd (17,000 ppm Pd). All scalebars are 500 nm.

7. X-Ray absorption spectroscopy (XAS) experiments

X-Ray absorption spectroscopy (XAS) was used to further characterise the metal clusters in P10 synthesized via a Suzuki-Miyaura polycondensation reaction and via Yamamoto coupling (P10Y). We studied as-synthesized P10 containing 8000 ppm Pd (similar to the 7000 ppm Pd sample discussed in the main manuscript), P10 containing 10,000 ppm Pd following photodeposition (derived from as-synthesized P10 with 2000 ppm Pd), and P10Y.

In the XAS data processing, the photon energy of the collected XAS spectra was calibrated at the first inflection point of the derivative XAS spectrum of Pd or Ni foil, and then normalized by Athena (version of 0.9.26) software. The backgrounds in the regions of pre-edge and polynomial post-edge in these sample XAS spectra were normalized by subtracting from the raw I_f/I_0 data (I_f: Intensity of reflected light projected on the filter in fluorescence mode; I_0: Intensity of initial light from light source). In addition, the extended X-ray absorption fine structure (EXAFS) spectra of these samples were mathematically converted to k^2-weighted in the region of 4.1-12.1 $Å^{-1}$. Subsequently, these k^2-weighted EXAFS spectra were Fourier-transformed (FT) to FT-EXAFS spectra to analyze the coordination configuration, including coordination number, bond distance, and Debye-Waller factor of Pd and Ni in samples. For the model fitting in Artemis software (version of 0.9.26), the crystal structure parameters of aforementioned palladium foil and several nickel standards for model fitting were downloaded from the online Inorganic Crystal Structure Database (ICSD) (https://icsd.fiz-karlsruhe.de/search/basic.xhtml).

With the aid of XAS spectra, the valence of Pd and Ni in samples can be identified by comparing their XAS spectra with that of other metal references. As shown in **Figure S9a**, the XAS spectra are composed of three parts, including pre-edge (-150 to -50 eV), edge/white line (-50 to 50 eV), and post-edge (50 to 250 eV) regions (The inflection point in edge region is set as the datum, 0 eV). The signal of edge/white line region in these XAS spectra is contributed to the electron excitation from 1*s* to 4*p* orbital which can be adopted for the valence identification for elements. However, the inflection point shift in these samples are unobvious in our case that can only identified with the feature variation of white line region, as shown in the inserted figure in **Figure S9a**. The sequence of white line intensity is P10-photodeposited>P10-synthesis proportional to their Pd amounts. Apart from Pd amount, the white line intensity is also proportional to the *d*-orbital empty and coordination number of Pd in samples. Therefore, the most Pd atoms in these P10 samples existed as the valence of Pd(0) and have the relatively lower coordination number compared with Pd foil, revealing that Pd atom is well-dispersed by P10 polymer. In addition, the higher absorption peak intensity at lower photon energy in the white line region also refers to the existence of oxidized Pd atoms.[4,5] That is, a few Pd atoms were bound with the oxygen atoms of P10 polymer, forming PdO_x-based clusters with a higher Pd valence. In order to obviously depict the photon energy position of inflection points in each of the samples for Pd valence identification, their first derivative normalized XANES spectra are shown with that of Pd foil in **Figure S9b**. The inflection point position of samples is basically located at 24350 eV which is same as that of Pd foil, implying that the average Pd valence in various samples is Pd(0). Furthermore, the coordination environment of Pd in these P10 samples and Pd foil were compared in forms of k^2-weighted XANES spectra, as displayed in **Figure S9c**. In the region of wavenumber higher than 2.5 $Å^{-1}$, the oscillation frequency of samples was same with that of Pd foil, suggesting that their Pd coordination environment was metal-like. Most particularly, the oscillation frequency of the P10 samples are higher than that of Pd foil in the region of wavenumber lower than 2.5 $Å^{-1}$. This oscillation frequency difference is possibly contributed by the intermolecular correlation between Pd and surrounding P10 polymer.

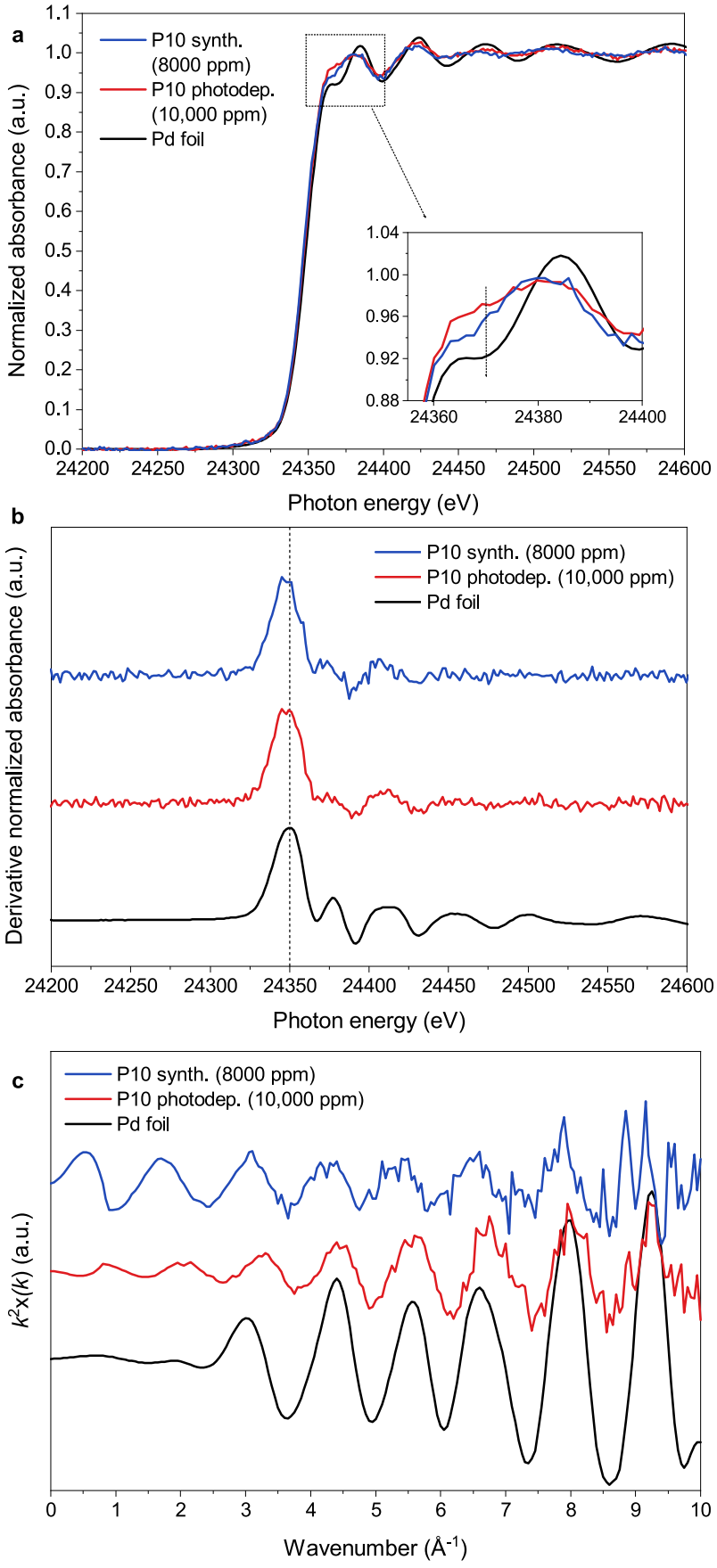

Figure S9. Pd *K*-edge **(a)** normalized and **(b)** derivative normalized X-ray absorption near-edge spectroscopy (XANES) spectra of samples and Pd foil reference. **(c)** k^2-weighted XANES.

Figure S10 exhibits the bond distance of first coordination shell, Pd-Pd in the studied P10 samples and in Pd foil. In comparison with Pd foil, the Pd-Pd intensity of the P10 samples were relatively lower (0.5-1.0 $Å^{-3}$) than that of Pd foil (~3.0 $Å^{-3}$) because of their lower Pd coordination number which can be ascribed to a P10 polymer dispersion effect. On the basis of this principle, the Pd coordination number of P10-Photodeposited was the highest among these samples. The coordination number and bond distance of Pd in samples were derived from the model-fitted FT-EXAFS spectra which show good agreement between fitting curve and FT-EXAFS spectra for the P10 samples and Pd foil, especially at the first shell, Pd-Pd. The model-fitting results of FT-EXAFS spectra for samples and Pd foil are summarized in **Table S2**. In comparison to Pd foil, the coordination number of Pd in the P10 samples were lower, indicating that the Pd atoms were well-dispersed by P10 polymer. With a lower Pd amount and a specific synthesis route, the P10 polymer can more effectively separate the Pd atoms, resulting to a lower coordination number with a longer Pd-Pd bond distance.

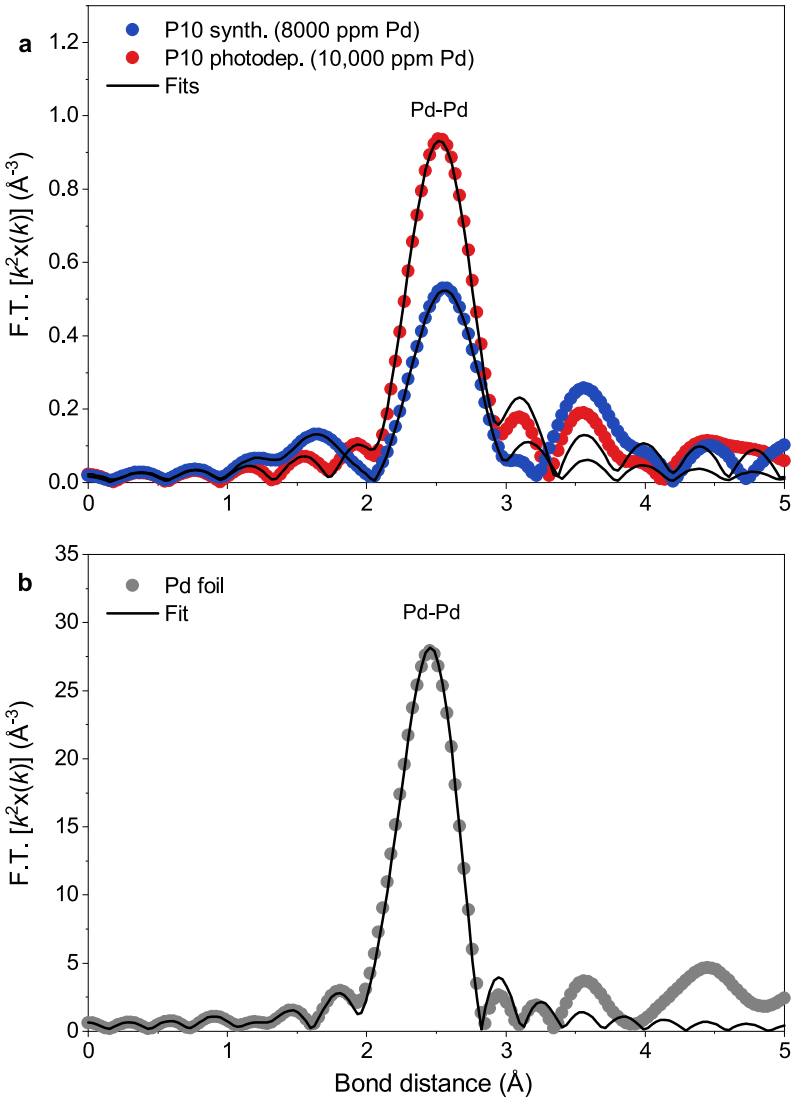

Figure S10. Fourier-transformed extended X-ray absorption fine structure spectra (FT-EXAFS), and model-fitted FT-EXAFS spectra of **(a)** P10 samples and **(b)** a Pd foil reference.

Table S2. Coordination number (CN), bond distance (R), and Debye-Waller factor (σ^2) of the P10 samples and the Pd foil reference as derived from model-fitted FT-EXAFS spectra.

Sample	1st Shell	CN	R (Å)	$\sigma^2 \times 10^3$ (Å^2)
P10 synth. (8000 ppm Pd)	Pd-Pd	3.30	2.55	9.05
P10 photodep. (10,000 ppm Pd)	Pd-Pd	7.72	2.52	11.96
Pd foil reference	Pd-Pd	8.65	2.45	5.39

In the case of P10Y a similar 3-D structure is observed, with Ni central atoms surrounding P10 polymer. **Figure S11a** displays the feature and the shift of inflection point in edge-jump region (inserted figure) position of P10Y as compared to those of Ni(II) references. The accurate inflection points of P10Y and nickel references are shown in the first derivative normalized XANES spectra in **Figure S11b**. It is apparent that the inflection point of P10Y was 8343.8 eV which was between that of Ni foil (8333.0 eV) and NiO (8345.5 eV). To precisely obtain the Ni valence in P10-Yamomoto, the linear regression line was derived from the inflection points of various nickel references with high R^2 value (> 0.980), as displayed in **Figure S11c**. The Ni valence in P10-Yamamoto was a lower mixed-valence, 1.906, suggesting that the existences of Ni(0) (4.7%) and Ni(II) (95.3%). Additionally, the coordination environment of Ni in P10-Yamomoto was compared with that of other nickel references in forms of k^2-weighted XANES spectra, as exhibited in **Figure S11d**. The oscillation frequency, amplitude, and feature of P10-Yamamoto were similar with those of Ni(II) species, especially $Ni(OH)_2$, implying a similar coordination environment.

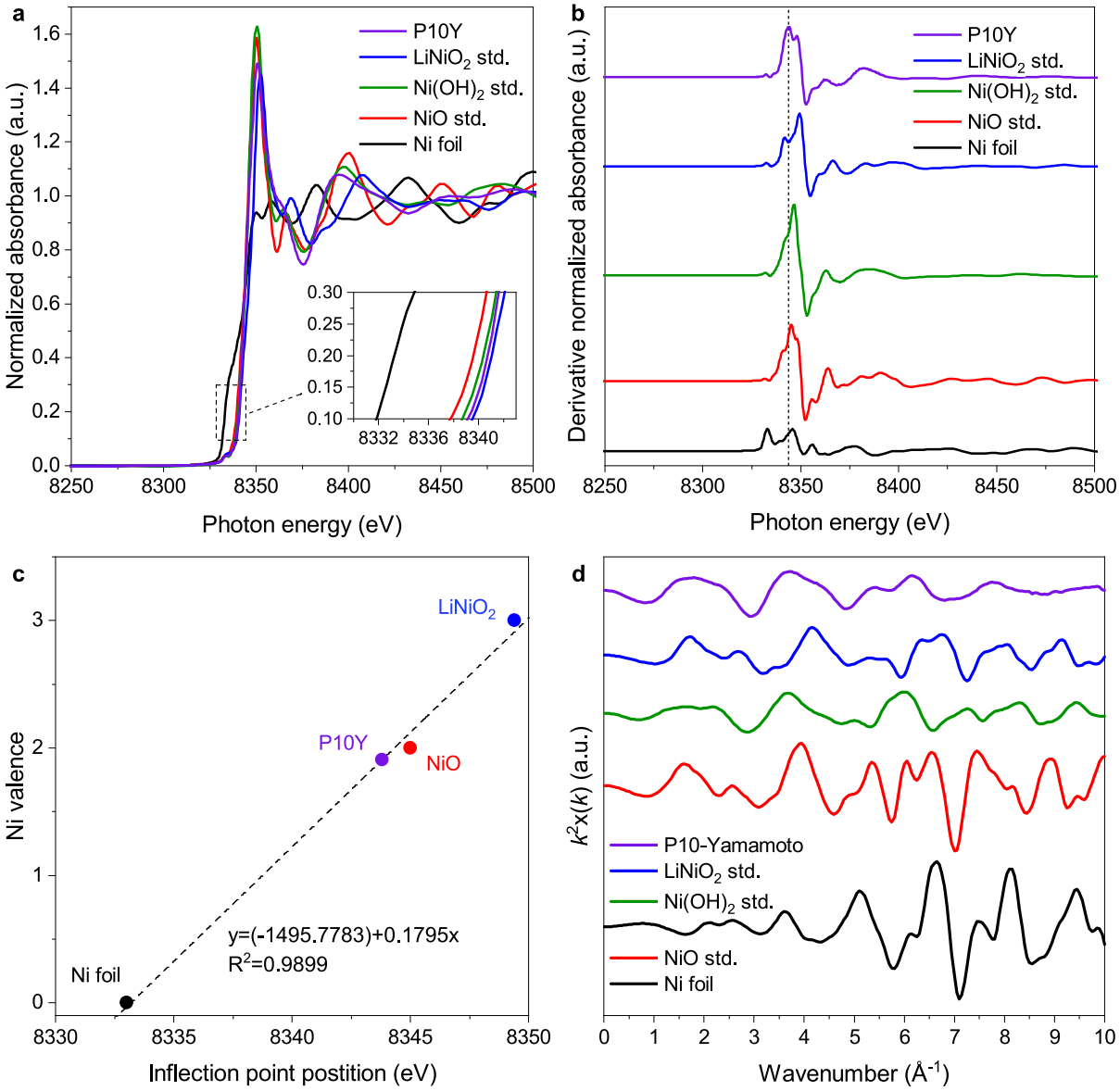

Figure S11. Ni *K*-edge **(a)** normalized and **(b)** first derivative XANES spectra of P10Y and Ni references. **(c)** Linear regression derived from nickel references for Ni valence identification in P10Y. **(d)** k^2-weighted XANES.

Figure S12 shows the coordination shells of P10Y and other nickel references. Among these nickel references, the feature of $Ni(OH)_2$ was near that of P10Y, especially in the first shell, Ni-O at 1.60 Å. The existence of Ni-O bond in first shell indicates the occurrence of interatomic bond formation between Ni and O atoms in P10 polymer. These Ni atoms and P10 polymers arranged into an six-coordinated octahedral structure similar with $Ni(OH)_2$. Regarding to the second shell, Ni-Ni at 2.27 Å, was approaching the bond distance of Ni-Ni in Ni foil, 2.18 Å. This may be attributed to the existence of a few Ni(0) atoms, which was consistent with the aforementioned results from XANES spectra.

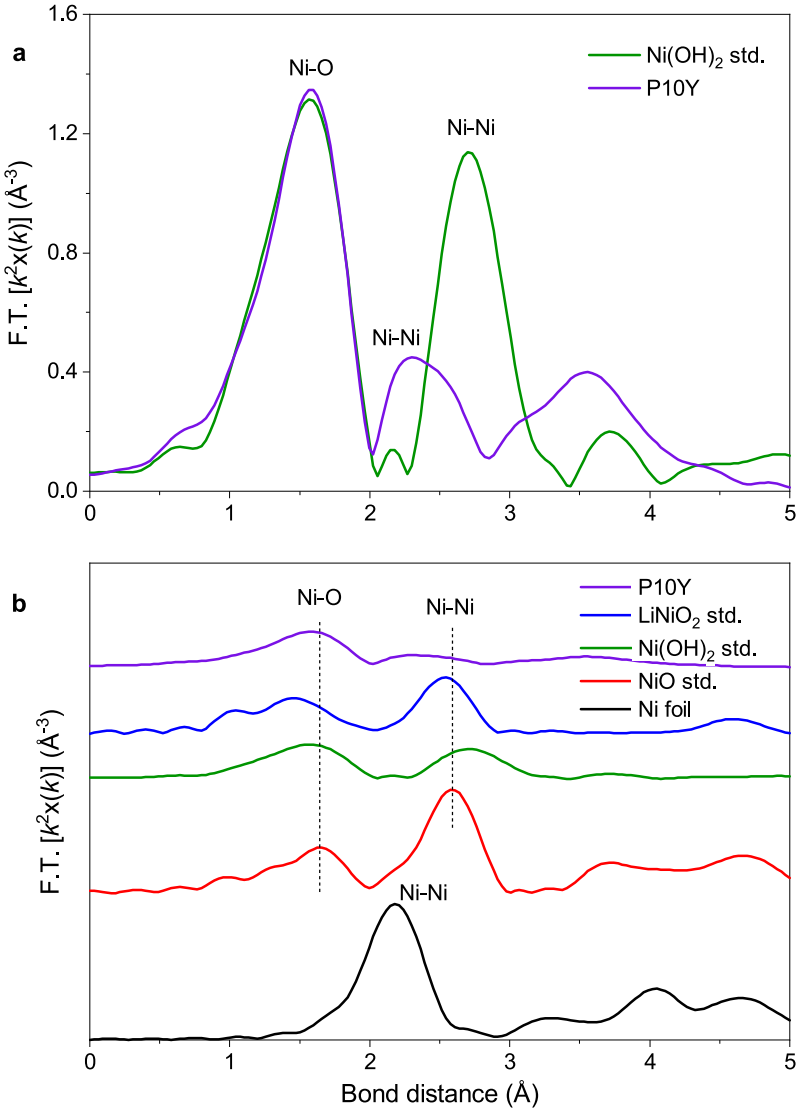

Figure S12. FT-EXAFS spectra of **(a)** P10Y and $Ni(OH)_2$ and **(b)** P10Y and all Ni references.

6. P10 with varying Pd content

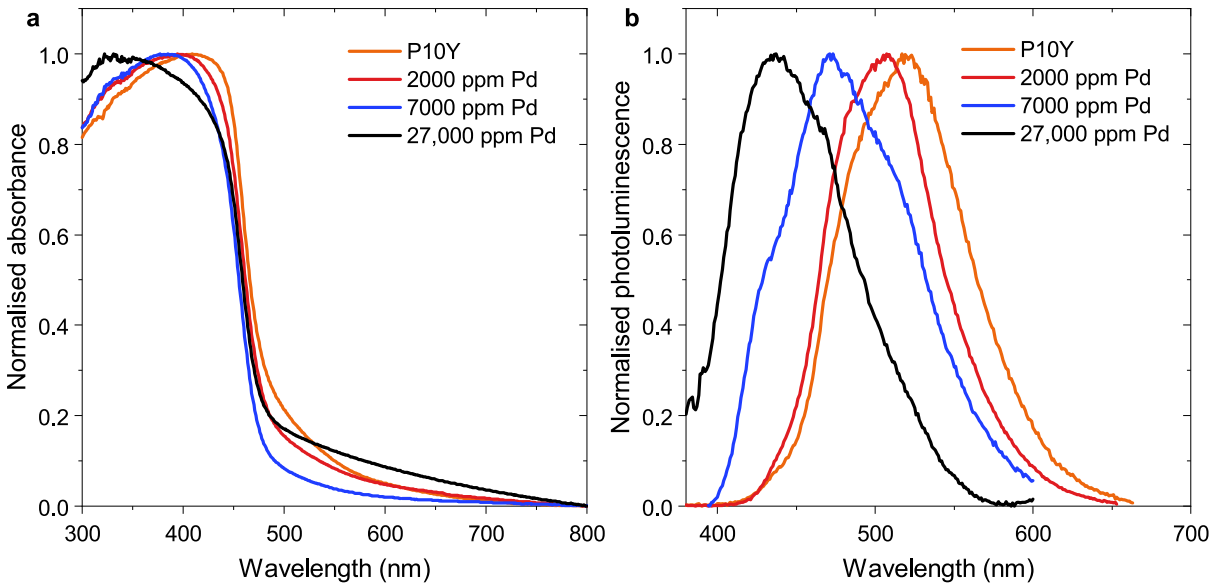

Figure S13. Steady-state optical properties of P10 with varying Pd content. **(a)** Solid state diffuse reflectance spectra and **(b)** photoluminescence emission spectra obtained upon 340 nm excitation of the different P10 batches.

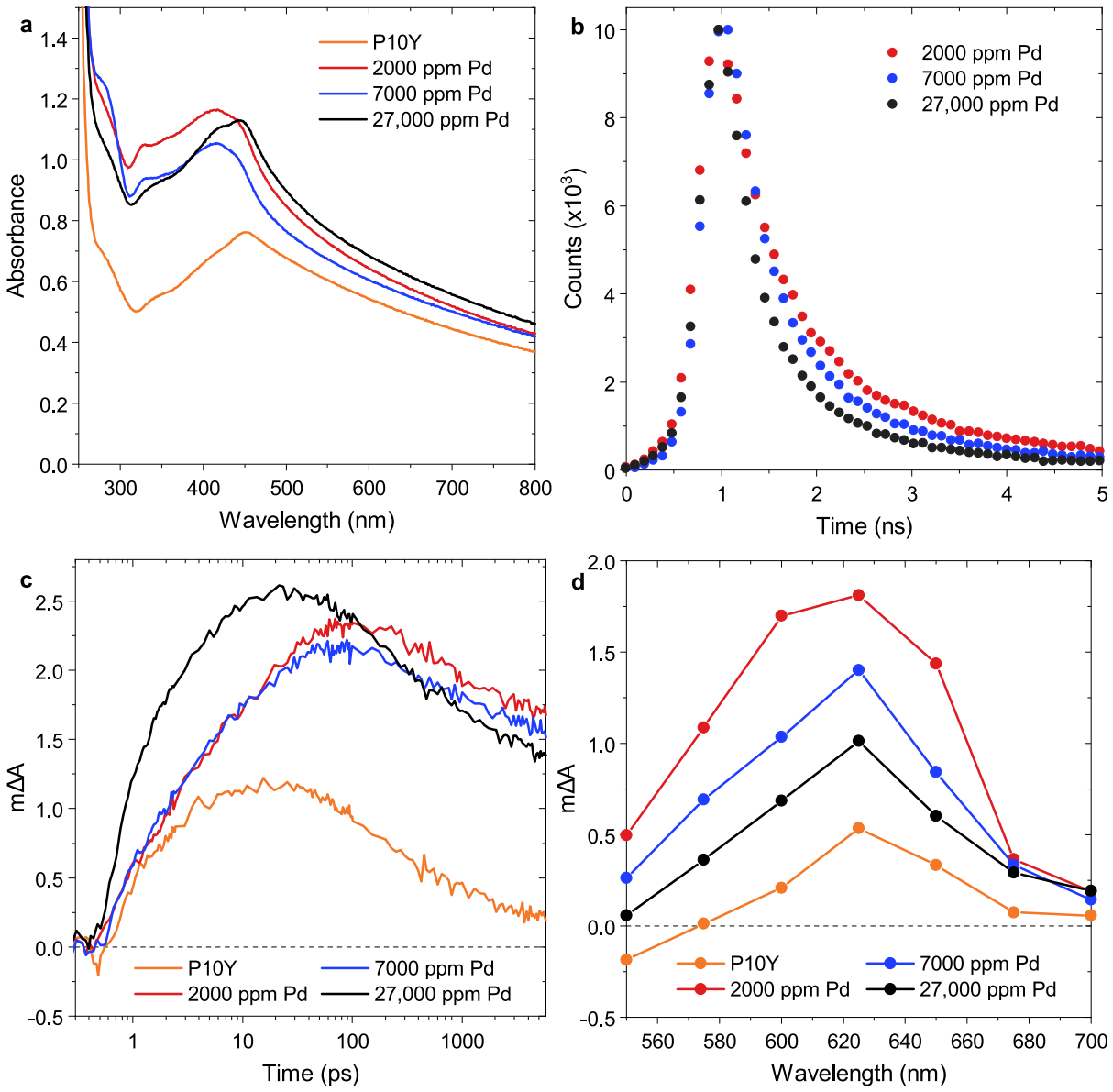

Figure S14. Steady-state absorbance and transient data on P10 particles with different Pd content, obtained in a solvent mixture consisting of equal volumes of H_2O/MeOH/TEA: **(a)** Steady state absorbance spectra in H_2O/MeOH/TEA recorded without an integrating sphere (unlike the one shown in Figure 1, thus exhibiting more scattering); **(b)** Fluorescence lifetime decays in the solid state, recorded with a fixed peak count of 10,000 counts. **(c)** transient absorption kinetics in H_2O/MeOH/TEA probed at 630 nm on the fs – early ns timescale following 355 nm excitation using a fluence of 0.08 mJ cm^{-2}; **(d)** transient absorption spectra in H_2O/MeOH/TEA probed at 10 μs following nm following 355 nm excitation using a fluence of 0.32 mJ cm^{-2}. All samples were prepared with a polymer concentration of 0.24 g L^{-1}. Note that the charge yield on the ps – ns timescale largely reflects the absorbance differences at the excitation wavelength between the different samples and

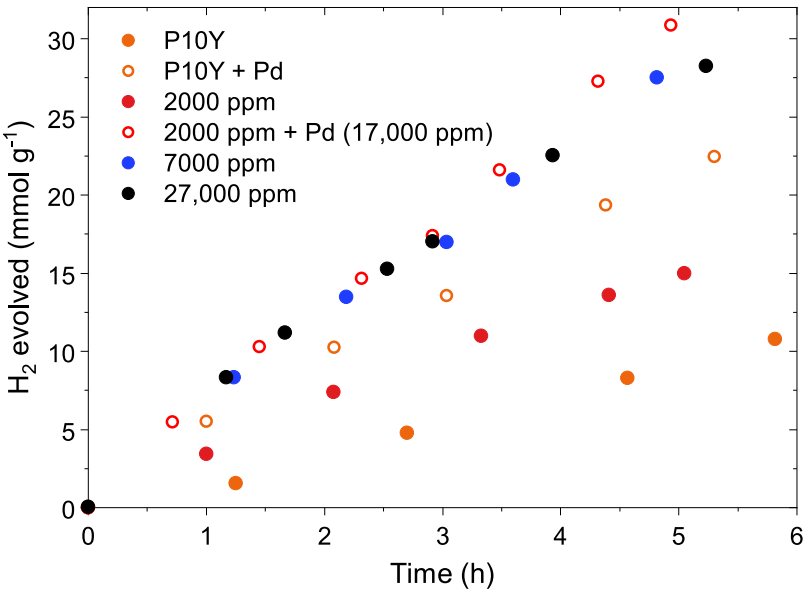

Figure S15. Photocatalytic testing of P10 samples with different Pd content. P10 (25 mg) was suspended in H_2O/MeOH/TEA (1:1:1, 25 mL) and sonicated for 10 minutes before degassing by N_2 bubbling. Samples were irradiated with a 300 W Xe lamp fitted with a $\lambda > 420$ nm filter. The samples with added Pd (orange and red open circles) were prepared via the same method but with the addition of 2 wt. % Pd to the sample, in the form of $Pd(NH_4)_2Cl_4$, before sonication.

References

(1) Cha, H.; Wheeler, S.; Holliday, S.; Dimitrov, S. D.; Wadsworth, A.; Lee, H. H.; Baran, D.; McCulloch, I.; Durrant, J. R. Influence of Blend Morphology and Energetics on Charge Separation and Recombination Dynamics in Organic Solar Cells Incorporating a Nonfullerene Acceptor. *Adv. Funct. Mater.* **2018**, *28* (3), 1704389.

(2) Collado-Fregoso, E.; Deledalle, F.; Utzat, H.; Tuladhar, P. S.; Dimitrov, S. D.; Gillett, A.; Tan, C.-H.; Zhang, W.; McCulloch, I.; Durrant, J. R. Photophysical Study of DPPTT-T/PC 70 BM Blends and Solar Devices as a Function of Fullerene Loading: An Insight into EQE Limitations of DPP-Based Polymers. *Adv. Funct. Mater.* **2017**, *27* (6), 1604426.

(3) Lewis, A. J.; Ruseckas, A.; Gaudin, O. P. M.; Webster, G. R.; Burn, P. L.; Samuel, I. D. W. Singlet Exciton Diffusion in MEH-PPV Films Studied by Exciton–Exciton Annihilation. *Org. Electron.* **2006**, *7* (6), 452–456.

(4) Grunwaldt, J.-D.; Caravati, M.; Ramin, M.; Baiker, A. Probing Active Sites During Palladium-Catalyzed Alcohol Oxidation in “Supercritical” Carbon Dioxide. *Catal. Letters* **2003**, *90* (3/4), 221–229.

(5) Caravati, M.; Grunwaldt, J.-D.; Baiker, A. Selective Oxidation of Benzyl Alcohol to Benzaldehyde in “Supercritical” Carbon Dioxide. *Catal. Today* **2004**, *91–92*, 1–5.